Unique patterns of CD8+ T cell-mediated organ damage in the Act-mOVA/OT-I model of acute graft versus host disease

Barbara Érsek[1,2,§], Nikolett Lupsa[1,2,§], Péter Pócza[3], Anett Tóth[1,2], Andor Horváth[1,2], Viktor Molnár[2,4], Bence Bagita[1,2], András Bencsik[1,2], Hargita Hegyesi[5], András Matolcsy[3], Edit I Buzás[2] and Zoltán Pós[1,2]

[1]Hungarian Academy of Sciences - Semmelweis University "Lendület" Experimental and Translational Immunomics Research Group, 1089 Budapest, Hungary, [2]Dept. of Genetics, Cell and Immunobiology, Semmelweis University 1089 Budapest, Hungary,[3]1st Department of Pathology and Experimental Cancer Research, Semmelweis University 1085 Budapest, Hungary, [4]Csertex Research Laboratory, 1037 Budapest, Hungary [5]"Frédéric Joliot-Curie" Inst. for Radiobiology and Radiohygiene, 1221 Budapest, Hungary

[§]These authors contributed equally to this work

Corresponding author: Zoltán Pós

E-mail address: pos.zoltan@med.semmelweis-univ.hu

Fax number: +36-1-303-69-86

Telephone number: +36-1-210-2930/56435 Ext.

Address: Hungarian Academy of Sciences - Semmelweis University "Lendület" Experimental and Translational Immunomics Research Group, Budapest, Hungary

4 Nagyvárad tér Budapest H-1089 Hungary

Funding

This work was supported by the Hungarian Academy of Sciences ("Lendület" LP2012-49/2012) and the Hungarian National Research, Development and Innovation Office (OTKA K 116340).

Acknowledgements

The authors would like to thank Tamás Masszi and András Falus for critical reading of the manuscript.

Abstract

T-cell receptor (TCR)-transgenic models of acute graft versus host disease (aGvHD) offer a straightforward and highly controlled approach to studying mechanisms and consequences of T-cell activation following allogeneic hematopoietic stem cell transplantation (aHSCT).

Here we report that aHSCT involving OT-I mice as donors, carrying an ovalbumin-specific CD8+ TCR, and Act-mOVA mice as recipients, expressing membrane-bound ovalbumin driven by the β-actin promoter, induces lethal aGvHD in a CD8+ T cell-dependent, highly reproducible manner, within 4-7 days. Tracking of UBC-GFP/OT-I graft CD8+ T-cells disclosed heavy infiltration of the gastrointestinal tract, liver and lungs at the onset of the disease, and histology confirmed hallmark features of gastrointestinal aGVHD, hepatic aGvHD, and aGvHD-associated lymphocytic bronchitis in infiltrated organs. However, T-cell infiltration was virtually absent in the skin, a key target organ of human aGvHD, and histology confirmed absence of cutaneous aGVHD, as well. We show that the model allows studying CD8+ T-cell responses in situ, as selective recovery of graft CD45.1/OT-I CD8+ T-cells from target organs is simple and feasible by automated tissue dissociation and subsequent cell sorting. Assessment of interferon-gamma production by flow cytometry, granzyme-B release by ELISA, TREC assay and whole genome gene expression profiling confirmed that isolated graft CD8+ T-cells remained intact, underwent clonal expansion and exerted effector functions in all affected tissues.

Taken together, these data demonstrate that the OT-I/Act-mOVA model is suitable to studying CD8+ T cell-mediated effector mechanisms in a disease closely resembling fatal human gastrointestinal and hepatic aGVHD that may develop after aHSCT using HLA-matched unrelated donors.

Keywords:

Experimental model, cytotoxic T cell, homing, CAG-OVA

Abbreviations

aGvHD	Acute graft versus host disease
aHSCT	Allogeneic hematopoietic stem cell transplantation
Act	Chicken beta actin promoter

APC	Antigen-presenting cell
CMV	Cytomegalovirus
CTL	Cytotoxic T lymphocyte
DEG	differentially expressed gene
ELISA	Enzyme-linked immunosorbent assay
FDR	False discovery rate
GFP	Green fluorescent protein
GI	Gastrointestinal
GSEA	Gene set enrichment analysis
HE	Hematoxylin-eosin staining
HUGO	Human Genome Organisation
IHC	Immunohistochemistry
K14	cytokeratin 14 promoter
miHA	minor histocompatibility antigen
mOVA	membrane-bound chicken ovalbumin
MUD	MHC-matched unrelated donor
NES	Normalized enrichment score
PBMC	Peripheral blood mononuclear cell
PDGF	Platelet-derived growth factor
sjTREC	Signal joint T cell receptor excision circles
sOVA	Soluble chicken ovalbumin
TBI	Total body irradiation
UBC	Human ubiqutin C promoter

Introduction

Acute graft versus host disease (aGvHD) is a common, life-threatening side effect of allogeneic hematopoietic stem cell transplantation (aHSCT). Acute GvHD is induced by various graft-derived immunocompetent cells, most prominently graft-derived naïve CD8+ and CD4+ T cells exerting cytotoxic effects on multiple organ systems of the allogeneic recipient upon activation by recipient APCs via presentation of various major and/or minor histocompatibility antigens[1]. Typical manifestations of aGvHD include widespread, graft-mediated organ damage most typically affecting the skin, gastrointestinal (GI) tract and liver, involving, among others, mobilization of the gut microbiota[2,3], consequent cytokine storm[4], and massive organ dysfunction that may lead to the demise of the patient[1,5].

Currently, the most frequently used murine models of human aGvHD utilize distinct, inbred mouse strains as allogenic donors and recipients to induce aGvHD upon experimental aHSCT[6-8]. This approach is highly efficient, as it achieves both major and minor allele disparities between donor and recipient, and evokes potent aGvHD mediated by graft CD8+ T cells, CD4+ T cells, or both[9,10]. However, as major allele (MHC) disparities are generally avoided in human clinical aHSCT, several murine models have been developed in that multiple minor allele disparities are present only [11-13]. Finally, a few novel murine aGVHD models have also been introduced based on single, well-defined minor histocompatibility allele recognized by a single, transgenic TCR present on all graft T cells, too[14-16].

Generally, utilization of a single minor antigen mismatch and a transgenic TCR has several advantages and allows a more straightforward analysis of T cell activation and T-cell-mediated effects in experimental aGVHD. This is because these models greatly reduce heterogeneity of antigen-specific effector T cell responses, efficiently decrease the number of non-specific effector T cells present in the activated T cell pool (i.e. bystander T cells activated by the cytokine storm), and also allow for a more straightforward result interpretation, as T cells react to a single, well-defined target antigen, the biological properties, expression patterns and bioavailability of which is exactly known. This is in marked contrast with multiple mismatch models in that availability of such information is limited at best.

Among the various aGvHD models based on transgenic TCRs and single miHA mismatch, the OT-I/K14-OVA model, originally reported by Shibaki et al [17]., is of major interest, as this model is based one of the arguably most extensively studied murine TCR / model antigen system. Here, a transgenic Tcra-V2/Tcrb-V5 T cell receptor, present on all graft CD8+ T cells (OT-I), recognizes a chicken ovalbumin$^{257-264}$ octapeptide epitope (SIINFEKL)

presented by the H2-K^b MHC I allele of both recipient APCs and parenchymal cells in typical target organs of the recipient (OVA). Shibaki et al. demonstrated [17] that K14-OVA mice expressing the chicken ovalbumin (OVA) antigen under the control of a cytokeratin 14 (K14) promoter develop aGvHD-like symptoms in the skin upon adoptive transfer of OT-I CD8+ T cells in a highly reproducible manner [17]. However, this model was not reported to develop other forms of aGvHD, such as GI, or hepatic aGvHD, which are typical manifestations of the equivalent human disease [18]. Second, this model did not require chemotherapy or total body irradiation (TBI) prior T cell grafting to induce aGvHD-like symptoms, which is also in contrast with most other murine aGvHD models and also human clinical aGvHD, in that organ damage caused by chemo and/or radiotherapy performed before transplantation is a major driving force of aGVHD [19].

Here we report that by replacing K14-OVA mice with Act-mOVA mice as recipients, and using TBI as conditioning regimen before grafting OT-I CD8+ T cells, a murine aGVHD model system can be created that still relies on the well-known OT-I/OVA model antigen recognition, but is arguably closer to human aGvHD and provides opportunity to study T cell responses in multiple target organ systems other than the skin, as well. We show that this approach induces severe, lethal aGvHD affecting the GI tract, liver and lungs of the recipients, but, interestingly, not the skin. As cutaneous and gastrointestinal aGvHD are two major modalities of the human disease, we suggest that the OT-I → Act-mOVA system may be used as a complementary model to the OT-I → K14-OVA system; the latter for studying a rather indolent disease course with cutaneous aGvHD, while the former for analyzing a more aggressive, severe lethal aGVHD involving massive internal organ damage instead.

Methods

Mice

Wild type C57BL/6J (B6 mice), C57Bl/6-Tg(CAG-OVA)-916Jen/J (hereafter termed as Act-mOVA), C57BL/6-Tg(TcraTcrb) 1100Mjb/J (hereafter termed as OT-I), B6.SJL-Ptprca Pepcb/BoyJ (hereafter referred to as CD45.1) and C57BL/6-Tg(UBC-GFP)30Scha/J (hereafter referred to as UBC-GFP) were purchased from The Jackson Laboratory (Bar Harbor, ME, USA). For some experiments, OT-I mice were backcrossed to the CD45.1 and UBC-GFP backgrounds (hereafter termed as OT-I/CD45.1, and OT-I/UBC-GFP mice, respectively). All animals were housed in IVC racks, on a 12L:12D cycle, and used at 10-16 weeks of age. All animal experiments were conducted with approval of the Institutional Animal Care and Use Committee.

OT-I → OVA acute GvHD model

CD8+ T cell-dependent acute GvHD was induced in healthy C57Bl/6 female mice by allogeneic hematopoietic stem cell transplantation (aHSCT). Briefly, on the day of aHSCT (aHSCT + Day 0), recipient mice received 11Gy total body irradiation in two split doses (5.5 Gy each), 3 hours apart, using a linear accelerator (1.07Gy/min). Irradiated animals were then transplanted with $3x10^6$ allogeneic bone marrow cells and $1.5x10^7$splenocytes via retroorbital injection, under ketamine-xylazine anesthesia. In most experiments, aGvHD was induced using OT-I mice as donors and Act-mOVA mice as recipients (OT-I → Act-mOVA model), both on the C57Bl/6 background. After aHSCT, mice were monitored daily for weight loss, hunchback, ruffled fur, apathy and (unless otherwise stated) euthanized on aHSCT + Day 4 by CO2 asphyxiation. For control experiments, recipient mice were also grafted with CD8+ T cell-depleted grafts (OT-I/CD8 depleted → Act-mOVA), CD8+ T cell-depleted grafts spiked with increasing numbers of OT-I T cells (OT-I → Act-mOVA), syngeneic grafts (Act-mOVA → Act-mOVA), or grafts with multiple minor and major histocompatibility antigen disparities (Balb/c → B6 aGvHD system).

Histology

For histological analysis, mice were sacrificed at the time points indicated, and the skin, small intestine, lungs and liver were removed. Next, 5 μm thick FFPE sections were prepared, and standard hematoxylin and eosin

staining was performed. Images were captured with an inverted microscope (DMI 6000B; Leica, Wetzlar, Germany) using a 10× objective in transmitted light mode. Tissue histology was evaluated by two independent pathologists.

Tracking UBC-GFP/OT-I CD8+ T cells in tissues affected by aGVHD

For T cell tracking, OT-I CD8+ T cells of the graft were replaced with UBC-GFP/OT-I CD8+ T cells. To this end, grafts were MACS-depleted of OT-I CD8+ T cells, and spiked with an equivalent number ($1{,}5x10^6$) of MACS-isolated UBC-GFP/OT-I T cells before aHSCT (Fig. 2). Grafts were then introduced in Act-mOVA mice and tissue samples were collected at various time points after aHSCT, as indicated. Next, tissue sections were prepared as above, mounted on SuperFrost Ultra Plus adhesive glass slides (GerhardMenzel, Braunschweig Germany), and boiled for antigen retrieval in sodium citrate buffer at ~+105 °C for 30 min. Endogenous peroxidase activity was blocked in 0.5 % hydrogen peroxide solution for 20 min. Finally, anti-GFP-HRP antibodies (1:200, Cell Signaling, Danvers, MA, USA) and the Novolink polymer kit (Leica) were used for detection of UBC-GFP/OT-I CD8+ T cells according to manufacturer's instructions. GFP-tagged cells were visualized using 3,3'-Diaminobenzidine (DAB) solution under microscopic control for 3–5 min. Slides were counterstained with hematoxylin.

Retrieval of CD45.1/OT-I CD8+ T cells by automated tissue dissociation and cell sorting

To retrieve grafted CD8+ OT-I T cells from bone marrow-transplanted OVA mice displaying acute GvHD, the CD45.1/OT-I → Act-mOVA aGvHD system was used (Fig. 4). CD45.2 OT-I T cells of the graft were replaced with CD45.1 OT-I T cells using selective CD8+ T cell depletion and spiking, as described above. On aHSCT + Day 4, mice were sacrificed to obtain the small intestine, lungs and liver, and tissue samples were dissociated using Miltenyi's Mouse Lamina Propria Dissociation, Mouse Lung Dissociation, and Mouse Tumor Dissociation kits (MiltenyiBiotec, Bergisch Gladbach, Germany), respectively, according to the manufacturer's instructions. Automated tissue dissociation was carried out on a Gentle MACS Octo Dissociator with Heating Upgrade (MiltenyiBiotec). Crude tissues lysates were subjected to 40%/80% Percoll gradient centrifugation (Sigma Aldrich, Seelze, Germany), graft CD45.1/OT-I CD8+ T cells were labeled with biotinylated anti-CD45.1 antibodies

(MiltenyiBiotec), anti-Biotin Microbeads, and retrieved by automated magnetic cell sorting using Miltenyi's AutoMACS Pro magnetic sorter ("posselds" program).

ELISA

For ELISA analysis, CD45.1/OT-I CD8+ T cells were collected from the grafts by MACS sorting, as above, on aHSCT + Day 0, before grafting, to serve as a reference. Next, on aHSCT + Day 4, grafted CD45.1/OT-I CD8+ T cells were also retrieved from the peripheral blood, small intestine, lungs and liver of Act-mOVA mice displaying acute GVHD by automated tissue dissociation and subsequent magnetic cell sorting, as above. Cells were plated on 96 well plates at a density of 10^4-10^5 cells/well, and cultured in RPMI-Glutamax supplemented by 10% FBS for 48 hours at +37°C in a 5% CO2 atmosphere. Culture supernatants were analyzed by a Mouse Granzyme B ELISA kit (Thermo Scientific) following the manufacturer's instructions. Granzyme B release was assessed using a Multiskan MS ELISA reader (Labsystems) and normalized to cell numbers.

TREC Assay

For TREC assays, CD45.1/OT-I CD8+ T cells were MACS sorted from the graft on aHSCT + Day 0, as controls. In addition, grafted CD45.1/OT-I CD8+ T cells were also retrieved from the peripheral blood, small intestine, lung and liver of transplanted Act-mOVA mice affected by acute GVHD on aHSCT + Day 4, as well. Genomic DNA was isolated from all MACS-sorted OT-I T cells using NucleoSpin Blood kits (Macherey-Nagel, Düren, Germany). Next, copy numbers of T-cell receptor excision circles (TRECs) were assessed by Q-PCR, as described elsewhere [20]. Briefly, primers and Taqman probes specifically designed for TREC assays performed on C57Bl/6 mice; i.e. forward: 5-CCAAGCTGACGGCAGGTTT-3; reverse: 5-AGCATGGCAAGCAGCACC-3; probe: FAM-5-TGCTGTGTGCCCTGCCCTGCC-3-TAMRA; (Microsynth, Balgach, Switzerland) were used to amplify TRECs. A standard reference copy number assay (transferrin receptor, Life Technologies) was used as internal reference. Amplifications were done using the Platinum Quantitative PCR Super Mix kits, a 7900 HT Fast RT PCR system (both from Life Technologies), and the following PCR protocol: +95°C for 10 min, and then +95°C 15 sec, +95°C 1 min for 45 cycles. Results were interpreted using the ddCt method.

Flow cytometry

Flow cytometry was performed using PE-Cy7 rat anti-mouse CD8b and (eBioscience), FITC mouse anti-mouse CD45.1 (MiltenyiBiotec), FITC mouse anti-mouse granzyme B (BioLegend, San Diego, CA, USA), and FITC rat anti-mouse IFN gamma (BD) antibodies. Cell viability was assessed with help of the LIVE/DEAD Fixable Dead Cell Stain Kit (Life Technologies). For intracellular staining, cell permeabilization was carried out using the Cytofix/Cytopermkit (BD). Data were collected on a FACS Calibur flow cytometer (BD) and analyzed by FlowJo (Tree Star Inc., Ashland, OR, USA).

Gene expression profiling

Total RNA was extracted from MACS-sorted CD45.1/OT-I CD8+ T cells using the RNeasy Plus Micro Kit (Qiagen, Valencia, CA). Sample integrity was analyzed on an Agilent 2100 Bioanalyzer (Agilent Technologies, Santa Clara, CA, USA). Next, 300pg of total RNA per sample was reverse transcribed, amplified in two rounds, and Cy3 labeled by the Arcturus RiboAmp PLUS, Cy3 labeling Kit (Life Technologies, Carlsbad, CA, USA). Amplified samples were hybridized to 4x44k mouse whole genome microarrays (Agilent) and scanned on an Agilent Microarray Scanner. Raw data were retrieved by the Feature Extraction software (Agilent), imported into GeneSpring (Agilent), quantile normalized, and the baseline was set to the median of all samples for every gene analyzed. Next, all genes flagged as not detected or not displaying signal intensities higher than the 20^{th} percentile of all detected signals in at least one experimental group were discarded. The remaining gene set was analyzed by principal component analysis (PCA) and further screened to identify differentially expressed genes (DEGs). To this end, any genes displaying >2 fold change between CD45.1/OT-I CD8+ T cells on aHSCT+ Day 0 (graft, serving a control) and any of the aGVHD-affected experimental groups on aHSCT + Day 4 (peripheral blood, small intestine, lungs and liver) were identified, and evaluated using One-Way ANOVA and Benjamini-Hochberg multiple testing correction ($p<0.05$). Within this gene set, Tukey's pairwise analysis was applied ($p<0.05$) to identify DEGs passing selection criteria in at least one of the four possible pairwise comparisons. This gene set was further analyzed by gene set enrichment analysis (GSEA), and select genes were also displayed on heatmaps generated by the Interactive Heatmap Viewer of the BRB-ArrayTools software. Raw microarray data have been deposited at the GEO database (GSE79083).

Statistics

Statistical analysis was done using GeneSpring (microarray studies) or the Graphpad software (all other analyses). One-Way ANOVA, Benjamini-Hochberg false discovery rate (FDR) correction and Tukey's all pairwise post hoc tests were used in all analyses. Unless otherwise stated, $P<0.05$ was considered statistically significant.

Results

Act-mOVA mice grafted with OT-I CD8+ T cells develop acute GvHD-like symptoms

Acute GvHD was induced by lethal dose TBI and subsequent aHSCT involving two transgenic, single minor allele-mismatched, but otherwise syngeneic mouse strains as aHSC donors and recipients. To this end, C57Bl/6 Act-mOVA mice (also known as CAG-OVA mice)[21] carrying an ubiquitously expressed membrane-bound chicken ovalbumin (OVA) transgene under control of the CMV immediate-early enhancer and chicken beta-actin promoter, and displaying the $OVA^{254-267}$ (SIINFEKL) peptide in the context of H2-K^b, were used as recipients, while C57Bl/6 OT-I animals[22], featuring CD8+ T cells with a transgenic TCR restricted to H2-K^b-presented SIINFEKL peptides were utilized as donors. Recipient mice were exposed to lethal dose TBI (11 Gy, in two split doses, 3 hours apart) and on the same day (aHSCT + Day 0), within 6 hours, grafted with donor-derived $3x10^6$ bone marrow cells and $1,5x10^7$splenocytes via retro-orbital infusion[23], thus resembling typical setups used in most standard murine aGVHD models [8]. In our hands, this approach, hereafter termed as the OT-I → Act-mOVA aGvHD model, induced well known hallmarks of mouse GvHD in recipient animals such as diarrhea, hunchback, ruffled fur and apathy. Typical onset of the symptoms was aHSCT + Day 2-3. Notably, extensive hair loss, reported in the K14-OVA model of aGVHD [17], was absent in the present system.

Act-mOVA mice grafted with OT-I CD8+ T cells develop lethal acute GvHD-like reaction in a highly reproducible fashion

Further, Act-mOVA animals grafted with OT-I CD8+ T cells displayed progressive weight loss (OT-I CD8+ → Act-mOVA Fig. 1A) and succumbed to the disease by aHSCT + Day 4-7 on average (median survival aHSCT + Day 5, OT-I CD8+ → Act-mOVA, Fig. 1B). In our hands, the reaction has been found highly reproducible as no animal was able to recover any weight lost, or survive beyond aHSCT + Day 8. Although lethal dose TBI for C57Bl/6 mice [7] was, as expected, sufficient to eliminate the host's bone marrow activity (Supplementary Fig. 1), the reaction observed was not a consequence of bone marrow failure; administration of syngraft bone marrow and splenocytes successfully rescued irradiated animals, resulting in nearly complete restoration of their original body weight by aHSCT + Day 14 (Act-mOVA → Act-mOVA, Fig. 1A, B). Nevertheless, like in human aGvHD, and unlike the K14-OVA a GvHD model, the reaction was dependent on TBI, as un-irradiated Act-mOVA animals

receiving identical grafts from OT-I mice did not develop any weight loss, symptoms of aGVHD, and survived without exception (not shown).

Lethal aGvHD-like reaction is CD8+ T cell-dependent and develops simultaneously to accumulation of CD8+ T cells in target organs

The lethal aGvHD-like reaction observed was fully CD8+ T cell-dependent, as MACS-depletion of OT-I CD8+ T cells from the graft (OT-I CD8 - → Act-mOVA, Fig. 1A, B), also rescued the hosts. The reaction was dependent on the number of grafted CD8+ OT-I T cells as well; spiking CD8+ T cell-depleted grafts with decreasing numbers of OT-I T cells gradually increased survival times (Fig. 1C). Generally, the reaction became unstable when administering very low numbers ($<10^2$) of immunocompetent OT-I T cells per graft (Fig. 1C, aHSCT + > Day 21 survival indicates complete recovery). When administering the full number of OT-I T cells, symptoms occurred with kinetics similar to those observed in the K14-OVA/OT-I model [17], but somewhat faster than in a standard aGvHD model[7] involving multiple MHC and minor allele mismatches between donors and similar, C57Bl/6 recipients (Balb/c→ C57Bl/6 Fig. 1A, B). Finally, in line with the notion that clonal expansion and immigration of CD8+ T cells into target tissues are instrumental in the induction of cytotoxic tissue damage in aGVHD reactions, we found gradual accumulation of CD8+ T cells in both the peripheral blood and also in typical target organs of aGVHD in recipient animals, such as the small intestine, liver and lungs (Fig. 1D). In most tissues, accumulation of CD8+ T cells plateaued on aHSCT + Day 4, the day preceding the time point of median survival (Fig. 1D). Interestingly, however, unlike in the K14-OVA model, the skin remained largely unaffected, as cutaneous infiltration by CD8+ T cells was not observed at any analyzed time points (Fig. 1D).

Cell tracking confirms that accumulation of CD8+ T cells in the organs affected is a graft-related phenomenon

As immigration of graft-derived CD8+ T cells into target organs is a hallmark feature of aGvHD, we next confirmed that accumulation of T cells is indeed graft-related, and not due to expansion of bystander T cells of the recipient that may survive TBI, and become activated by the consequent cytokine storm. By replacing OT-I CD8+ T cells of the graft with their UBC-GFP counterparts (Fig. 2A) we found that although affected organs contained substantial

numbers of bystander, UBC-GFP neg. CD8+ T cells of the host, accumulation of CD8+ T cells was indeed due to increasing numbers of graft-derived, UBC-GFP pos. OT-I CD8+ T cells (Fig. 2B).

Histology confirms heavy infiltration by graft CD8+ T cells and identifies hallmark features of aGvHD in all affected organs

We next analyzed whether the model was capable of evoking hallmark features of aGVHD pathology in affected organs. As CD8+ T cell infiltration reached peak levels on aHSCT + Day 4, this time point was selected for further analyses. Histology confirmed that in contrast to aHSCT + Day 0 (Fig. 3 A), by aHSCT + Day 4 (Fig. 3 B) extensive organ damage and severe villous atrophy were present in the small intestine. In addition, bile duct damage, lymphocytic infiltration of the portal tract and endotheliitis were prominent in the liver. Finally, severe lymphocytic bronchitis and alveolitis were observed in the lungs of affected animals (Fig. 3A, B). Parallel to this, numbers of UBC-GFP pos. graft CD8+ OT-I T cells reached their maximum, with strong CD8+ T cell infiltration present in all affected tissues, as visualized by GFP-specific IHC (Fig 3A, B). In marked contrast, histology of the skin showed endotheliitis but remained otherwise virtually unchanged; no subepidermal vesicle formation or separation of the epidermis and dermis was observed, apoptotic keratinocytes were not present in hair follicles, and in line with this, infiltration of UBC-GFP pos. graft CD8+ OT-IT cells in the dermis was virtually absent. Collectively, these data suggest that animals are affected by gastrointestinal and hepatic aGvHD, and also develop symptoms resembling human aGvHD-associated pulmonary bronchitis in the lungs, however, classic aGvHD of the skin is absent.

Intact graft CD8+ OT-I T cells can be retrieved from aGvHD-affected organs by automated tissue dissociation and cell sorting

We next tested whether CD8+ T cells mediating aGVHD can be retrieved from affected organs for analyzing CD8+ T cell activation and CTL-mediated effector mechanisms in these tissue environments. As we found that in spite of the lethal dose TBI, a significant number of UBC-GFP neg. CD8+ T cells of the recipient were still present in the affected tissues by aHSCT + Day 4, we retrieved bystander-free graft T cells for further analyses. To this end, we used CD45.1/OT-I CD8+ T cells to discriminate between graft-derived CD45.1+ CD8+ OT-I T cells and recipient

CD45.2+ CD8+ T cells or any other cells of the graft, and thereby ensure selective recovery of the former only (Fig. 5A). By applying automated tissue dissociation and automated magnetic sorting to recover CD45.1/OT-I CD8+ T cells on aHSCT + Day 4, we found that this approach yielded in substantial numbers of highly pure graft CD8+ T cells from the small intestine, lung, liver and peripheral blood in a highly reproducible manner (Fig. 5 B).

Graft CD45.1/OT-I CD8+ T cells retrieved from a GvHD-affected organs are enriched in activated cytotoxic effector T cells and display markers of clonal expansion

We next analyzed whether accumulation of CD45.1/OT-I CD8+ T cells is due to active homing of clonally expanded activated CD8+ effector T cells exerting cytotoxic effector functions, or rather passive recruitment of unstimulated resting graft CD8+ T cells to inflamed tissues with no CTL activity. First we found that CD45.1/OT-I CD8+ T cells infiltrating the organs affected by aGvHD produce granzyme B; this held true in both peripheral blood and the small intestine, lungs and liver (Fig. 5 C). Interestingly though, IFN-γ production was increased in circulating CD45.1/OT-I CD8+ T cells, but not in CD45.1/OT-I CD8+ T cells recovered from target organs (Fig 5 C). Next we tested whether recovered cells not only synthesize but also actively release granzyme B; we found that in contrast to aHSCT + Day 0, there was a massive (10-1000-fold) increase in the granzyme B release of grafted CD45.1/OT-I CD8+ T cells by aHSCT + Day 4 (Fig. 5 D). Finally, we also found that per cell numbers of T cell receptor excision circles (TRECs) showed a large drop (to about 1-10% of original TREC numbers) from aHSCT + Day 0 to aHSCT + Day 4 (Fig. 5 E), confirming that graft CD45.1/OT-I CD8+ T cells underwent clonal expansion typically observed upon losing naïve phenotype in CD8+ T cells [24]. Collectively, these data confirm that by aHSCT + Day 4, grafted CD45.1/OT-I CD8+ T cells underwent naïve to effector T cell transition, clonal expansion, and represent armed CD8+ effector T cells with cytotoxic activity in all analyzed organs affected by aGvHD.

Transcriptome profiling of graft CD8+ T cells confirms naïve to effector transition and discloses slight differences between CD8+ Teff cells infiltrating distinct target organs of aGvHD

Transcriptome profiling also confirmed that within four days after aHSCT, graft CD45.1/OT-I CD8+ T cells underwent major phenotypic changes in Act-mOVA recipients. First, Principal Component Analysis (PCA) showed that CD45.1/OT-I CD8+ T cells recovered from various organs of aGVHD-affected Act-mOVA animals on aHSCT +

Day 4 clustered closely together (Fig 6 A, red, green, grey, brown dots), clearly distancing themselves from CD45.1/OT-I CD8+ T cells on aHSCT + Day 0 (Fig 6 A, blue dots). According to PCA, the first two principal components of sample variance, i.e. the two most relevant factors creating differences between the analyzed T cell groups were attributable to the transcriptome-wide separation of T cells on aHSCT + Day 4 and aHSCT + Day 0 and, collectively exceeding 60% of total sample variance (Fig 6 A, Z axis, X axis). We next analyzed the exact molecular makeup of this difference by One-Way ANOVA and Benjamini-Hochberg corrections for multiple testing (false discovery rate <0.05) followed by Tukey's pairwise post hoc comparisons ($p<0.05$). When comparing CD45.1/OT-I CD8+ T cells isolated on aHSCT + Day 0, from the graft, with CD45.1/OT-I CD8+ T cells recovered from various organs affected by aGVHD on HSCT + Day 4, we found a total of 2514 differentially expressed genes (DEGs) discriminating between them (Supplementary Table 1). Among these genes we found several down-regulated markers associated with naïve CD8+ T cell phenotype (Fig. 6 B, top, e.g. FOXP1), markers typically lost upon differentiation to effector CD8+ T cells (CD7), or genes involved in the stabilization of memory CD8+ T cells rather than effector CTLs upon T cell activation (IL15RA). On the other hand, the data confirmed that upregulation of a large array of genes serving as makers of activated effector CTLs also took place. This latter group included known effector molecules of activated CD8+ effector T cells (Fig. 6 B, bottom, IFNG, GZMB, FASL), various cyclins (CCNA1, CCNB1, CCNB2, CCNE1, CCNG2) and DNA-polymerase subunits (POLA1, POLG2, POLM) linked to clonal expansion, genes supporting effector CTL expansion and survival (IL2RA, IL2RB), or genes upregulated in short-lived CD8+ effector T cells (PERP, Fig. 6 B). Finally, gene set enrichment analysis (GSEA) also confirmed that this difference is due to the fact that by aHSCT + Day 4, graft CD8+ T cells acquired an effector phenotype. GSEA disclosed that the majority of significant DEGs were particularly and significantly enriched in the topmost and bottommost sections of several canonical gene sets of the MSig database, ordered by direction and magnitude of change, discriminating between naïve and effector CD8+ T cells (Fig. 6C).

Interestingly though, we also found that the model may be sensitive enough to provide insight into tissue-specific differences in the functional properties of CD8+ T cells during aGvHD, as well. Apparently, in the small intestine, a large gene cluster of IL2R subunits and several cyclins, both closely linked with each other and associated with rapid clonal expansion following T cell activation, are less intensively transcribed than in any other target organ of aGvHD (Fig 6B, yellow frame). At this sample size the difference does not reach statistical significance, and an in-depth analysis of tissue-specific differences in the phenotype of CD8+ T cells infiltrating different organs in

aGVHD was beyond the scope of the present study. Still, coordinated dysregulation of such closely linked genes in T cells infiltrating a given tissue environment is interesting, as several lines of evidence indicate that differences exist in the phenotype of CTLs homing to different tissues affected by aGVHD[25,26], and some tissue-specific differences affect some specialized compartments of the CD8+ T cell memory[27], as well.

Discussion

In this study we describe a robust experimental model of aGvHD based on two commercially available transgenic mouse strains, capable of inducing highly reproducible, lethal aGvHD, to our best knowledge in 100% of the recipient animals, rapidly, within approximately 4-7 days.

The model is based on others' earlier work[17] showing that a minor allele mismatched, TCR-transgenic model of cutaneous aGvHD may be established by adoptive transfer of OT-I CD8+ T cells into keratin 14-OVA mice. Our data show that replacement of K14-OVA animals with Act-mOVA mice as recipients, and introducing TBI as conditioning regimen before aHSCT, have deep consequences on the disease course affecting both organ involvement and survival of the host. We found that in contrast to K14-OVA mice, lethally irradiated Act-mOVA animals develop widespread tissue damage affecting multiple organ systems[28], with histopathologic features closely resembling those of acute human gastrointestinal GvHD, hepatic GvHD, and GvHD-related lymphocytic bronchitis, respectively, and rapidly succumb to the disease. This is interesting not only because of the wider spectrum of organ involvement and more rapid progression to terminal disease, but also because the exact mechanisms and driving forces of aGvHD-associated lung damage are not particularly well documented [29-31], and hence this simplified model system may contribute to their better understanding, as well.

One of the key factors creating differences between the disease courses observed in the K14- and the Act-mOVA models is most probably the broader expression of the target antigen in the latter. Certainly, in a minor allele-mismatched, TCR-transgenic aGvHD model, linking the target antigen to a CMV enhancer-chicken beta actin promoter, being active in most cell types, rather than the keratin 14 promoter, being mostly active in epithelial cells and the skin, may allow induction of aGVHD in tissue environments other than the skin, as well[32].

Considering this, however, it is intriguing that in contrast to the K14-OVA model, the Act-mOVA system was not capable of developing cutaneous aGvHD at all. Certainly, none of the currently available murine GvHD models recapitulates all aspects and manifestations of the human disease. Still, it seems perplexing that such a ubiquitously expressed miHA does not generate T cell responses and aGVHD in such an accessible organ of the host. In fact, it had been convincingly shown that m-Act OVA skin contains chicken ovalbumin mostly in epithelial cells and hair follicles[21], the former of which are known targets in aGvHD. Also, both the K14- and the Act-mOVA models utilize membrane bound ovalbumin (mOVA) and not its soluble form (sOVA), with mOVA being easier to process for cross-presentation by local APCs of the host[33], the main inducers of T cell responses in

aGVHD. Finally, after Act-m OVA mice had been introduced to study T cell-mediated rejection mechanisms in solid organ transplantation, it was convincingly shown the skin grafts of Act-mOVA mice can be rejected by OT-I CD8+ T cells in the recipients [21].

On the other hand, however, the two systems differ in an additional aspect, namely the molecular context of the target antigen, too. In the K14-OVA animals used by Shibaki et al, OVA is present as a fusion protein linked to the PDGF receptor[34], while in Act-mOVA mice, OVA is coupled to an MHC-I transmembrane domain[21]. Such differences may seem irrelevant, but in fact have been shown to affect efficiency of antigen presentation and availability of MHC-linked antigenic peptides in aGvHD. Indeed, these factors are often more critical than the gross amount of the target antigen in an organ itself[35]. In fact there is evidence that the key to the above conundrum lies in differences in the efficiency of antigen presentation in the skin. It has been reported that in solid organ transplantation experiments, rejection of Act-mOVA skin transplants by OT-I CD8+ T cells is a rather long process (15-30 days) [21], far longer than that of K5-mOVA transgenic skin grafts by OT-I CD8+ T cells (8 days) [36], or that of most skin transplants by an MHC and minor allele mismatched allogeneic recipient (depending on model, 10—15 days) [37]. It has been suggested that delayed rejection of Act-mOVA skin grafts by CD8+ T cells is most probably due to limited availability of OVA-loaded APCs in the skin of Act-mOVA mice. Considering that in our system, aGvHD leads to the demise of the host within 4-5 days, and even with extremely reduced CD8+ T cell numbers, does not take not more than 10-14 days, we believe that the lack of cutaneous symptoms is due to the fact that the animals succumb to aGvHD before cutaneous symptoms may develop at all. Taken together, considering that the Act-mOVA model did not induce aGvHD in the skin, it certainly may not be considered as a model superior, but rather complementary to the K14-OVA system. It seems that the K14-OVA model induces a nonlethal, indolent, cutaneous disease, while the Act-mOVA approach recapitulates rather the gastrointestinal and some closely linked manifestations of an aggressive, fatal aGvHD. Cutaneous and gastrointestinal GvHD are the two main manifestations of human disease. They may occur both simultaneously and separately, both are of key importance in terms of disease prognosis, treatment of choice, and patient survival[18]. Hence, we believe that inducing them using the same TCR-transgenic donor but in two separate recipients (i.e. K14-OVA and Act-mOVA mice) may be a straightforward strategy to compare the two disease modalities, or even mechanisms of skin- and gut-directed homing of CD8+ T cells in aGvHD, within a highly controlled experimental environment.

Finally, it is worth noting that in the present model, aGvHD develops based on recognition of a sole minor antigen by a single transgenic TCR. This approach has several known advantages and drawbacks. First, this setup closely resembles situations of human aGvHD occurring as a consequence of aHSCT involving HLA-matched unrelated donors (MUD transplantation). Clearly, MUD transplantations occur in the majority of all human aHSCTs, hence the model is functionally often more relevant, than traditional models based on multiple disparities, involving a large and often undocumented array of minor and major antigen mismatches between donor and recipient. Also, with some modifications, this approach may be used to analyze antigen cross-presentation[16] or graft vs. leukemia effect, as well, as it has been shown elsewhere[38]. Nevertheless, the downside of this approach that due to its very nature, it is highly simplistic, relies mostly on CD8+ T cell activation, is limited to a single mismatched antigen, and hence even if it accurately depicts CD8+ T cell activation, it certainly does not recapitulate the full complexity of human aGvHD [39]. Interestingly however, as shown here, on the example of a large cluster of proliferation-associated genes differentially expressed by gut-homing graft T cells, even this simplified approach may provide valuable insight into the disease mechanism, such as differences in the CTL phenotype displayed in distinct target organs of aGvHD [26,25].

Disclosure

The authors declare that they have no conflict of interest.

References

1. Blazar BR, Murphy WJ, Abedi M (2012) Advances in graft-versus-host disease biology and therapy. Nat Rev Immunol 12 (6):443-458. doi:10.1038/nri3212

2. Jenq RR, Ubeda C, Taur Y, Menezes CC, Khanin R, Dudakov JA, Liu C, West ML, Singer NV, Equinda MJ, Gobourne A, Lipuma L, Young LF, Smith OM, Ghosh A, Hanash AM, Goldberg JD, Aoyama K, Blazar BR, Pamer EG, van den Brink MR (2012) Regulation of intestinal inflammation by microbiota following allogeneic bone marrow transplantation. J Exp Med 209 (5):903-911. doi:10.1084/jem.20112408

3. Holler E, Butzhammer P, Schmid K, Hundsrucker C, Koestler J, Peter K, Zhu W, Sporrer D, Hehlgans T, Kreutz M, Holler B, Wolff D, Edinger M, Andreesen R, Levine JE, Ferrara JL, Gessner A, Spang R, Oefner PJ (2014) Metagenomic analysis of the stool microbiome in patients receiving allogeneic stem cell transplantation: loss of diversity is associated with use of systemic antibiotics and more pronounced in gastrointestinal graft-versus-host disease. Biol Blood Marrow Transplant 20 (5):640-645. doi:10.1016/j.bbmt.2014.01.030

4. Ferrara JL (1993) Cytokine dysregulation as a mechanism of graft versus host disease. Curr Opin Immunol 5 (5):794-799

5. Hu SW, Cotliar J (2011) Acute graft-versus-host disease following hematopoietic stem-cell transplantation. Dermatol Ther 24 (4):411-423. doi:10.1111/j.1529-8019.2011.01436.x

6. Reddy P, Ferrara JLM (2008) Mouse models of graft-versus-host disease. In: StemBook. Cambridge (MA). doi:10.3824/stembook.1.36.1

7. Reddy P, Negrin R, Hill GR (2008) Mouse models of bone marrow transplantation. Biol Blood Marrow Transplant 14 (1 Suppl 1):129-135. doi:10.1016/j.bbmt.2007.10.021

8. Schroeder MA, DiPersio JF (2011) Mouse models of graft-versus-host disease: advances and limitations. Dis Model Mech 4 (3):318-333. doi:10.1242/dmm.006668

9. Rolink AG, Pals ST, Gleichmann E (1983) Allosuppressor and allohelper T cells in acute and chronic graft-vs.-host disease. II. F1 recipients carrying mutations at H-2K and/or I-A. J Exp Med 157 (2):755-771

10. van Leeuwen L, Guiffre A, Atkinson K, Rainer SP, Sewell WA (2002) A two-phase pathogenesis of graft-versus-host disease in mice. Bone Marrow Transplant 29 (2):151-158. doi:10.1038/sj.bmt.1703328

11. Korngold R, Sprent J (1978) Lethal graft-versus-host disease after bone marrow transplantation across minor histocompatibility barriers in mice. Prevention by removing mature T cells from marrow. J Exp Med 148 (6):1687-1698

12. Korngold R (1992) Lethal graft-versus-host disease in mice directed to multiple minor histocompatibility antigens: features of CD8+ and CD4+ T cell responses. Bone Marrow Transplant 9 (5):355-364

13. Toubai T, Tawara I, Sun Y, Liu C, Nieves E, Evers R, Friedman T, Korngold R, Reddy P (2012) Induction of acute GVHD by sex-mismatched H-Y antigens in the absence of functional radiosensitive host hematopoietic-derived antigen-presenting cells. Blood 119 (16):3844-3853. doi:10.1182/blood-2011-10-384057

14. Yu XZ, Albert MH, Anasetti C (2006) Alloantigen affinity and CD4 help determine severity of graft-versus-host disease mediated by CD8 donor T cells. J Immunol 176 (6):3383-3390

15. Albert MH, Liu Y, Anasetti C, Yu XZ (2005) Antigen-dependent suppression of alloresponses by Foxp3-induced regulatory T cells in transplantation. Eur J Immunol 35 (9):2598-2607. doi:10.1002/eji.200526077

16. Wang X, Li H, Matte-Martone C, Cui W, Li N, Tan HS, Roopenian D, Shlomchik WD (2011) Mechanisms of antigen presentation to T cells in murine graft-versus-host disease: cross-presentation and the appearance of cross-presentation. Blood 118 (24):6426-6437. doi:10.1182/blood-2011-06-358747

17. Shibaki A, Sato A, Vogel JC, Miyagawa F, Katz SI (2004) Induction of GVHD-like skin disease by passively transferred CD8(+) T-cell receptor transgenic T cells into keratin 14-ovalbumin transgenic mice. J Invest Dermatol 123 (1):109-115. doi:10.1111/j.0022-202X.2004.22701.x

18. Dignan FL, Clark A, Amrolia P, Cornish J, Jackson G, Mahendra P, Scarisbrick JJ, Taylor PC, Hadzic N, Shaw BE, Potter MN, Haemato-oncology Task Force of British Committee for Standards in H, British Society for B, Marrow T (2012) Diagnosis and management of acute graft-versus-host disease. Br J Haematol 158 (1):30-45. doi:10.1111/j.1365-2141.2012.09129.x

19. Turner BE, Kambouris ME, Sinfield L, Lange J, Burns AM, Lourie R, Atkinson K, Hart DN, Munster DJ, Rice AM (2008) Reduced intensity conditioning for allogeneic hematopoietic stem-cell transplant determines the kinetics of acute graft-versus-host disease. Transplantation 86 (7):968-976. doi:10.1097/TP.0b013e3181874787

20. Broers AE, Meijerink JP, van Dongen JJ, Posthumus SJ, Lowenberg B, Braakman E, Cornelissen JJ (2002) Quantification of newly developed T cells in mice by real-time quantitative PCR of T-cell receptor rearrangement excision circles. Exp Hematol 30 (7):745-750

21. Ehst BD, Ingulli E, Jenkins MK (2003) Development of a novel transgenic mouse for the study of interactions between CD4 and CD8 T cells during graft rejection. Am J Transplant 3 (11):1355-1362

22. Hogquist KA, Jameson SC, Heath WR, Howard JL, Bevan MJ, Carbone FR (1994) T cell receptor antagonist peptides induce positive selection. Cell 76 (1):17-27

23. Yardeni T, Eckhaus M, Morris HD, Huizing M, Hoogstraten-Miller S (2011) Retro-orbital injections in mice. Lab Anim (NY) 40 (5):155-160. doi:10.1038/laban0511-155

24. Gattinoni L, Lugli E, Ji Y, Pos Z, Paulos CM, Quigley MF, Almeida JR, Gostick E, Yu Z, Carpenito C, Wang E, Douek DC, Price DA, June CH, Marincola FM, Roederer M, Restifo NP (2011) A human memory T cell subset with stem cell-like properties. Nat Med 17 (10):1290-1297. doi:10.1038/nm.2446

25. Waldman E, Lu SX, Hubbard VM, Kochman AA, Eng JM, Terwey TH, Muriglan SJ, Kim TD, Heller G, Murphy GF, Liu C, Alpdogan O, van den Brink MR (2006) Absence of beta7 integrin results in less graft-

versus-host disease because of decreased homing of alloreactive T cells to intestine. Blood 107 (4):1703-1711. doi:10.1182/blood-2005-08-3445

26. Tsuchiyama J, Yoshino T, Saito T, Furukawa T, Ito K, Fuse I, Aizawa Y (2009) Cutaneous lymphocyte antigen-positive T cells may predict the development of acute GVHD: alterations and differences of CLA+ T- and NK-cell fractions. Bone Marrow Transplant 43 (11):863-873. doi:10.1038/bmt.2008.392

27. Mackay LK, Rahimpour A, Ma JZ, Collins N, Stock AT, Hafon ML, Vega-Ramos J, Lauzurica P, Mueller SN, Stefanovic T, Tscharke DC, Heath WR, Inouye M, Carbone FR, Gebhardt T (2013) The developmental pathway for CD103(+)CD8+ tissue-resident memory T cells of skin. Nat Immunol 14 (12):1294-1301. doi:10.1038/ni.2744

28. Wysocki CA, Panoskaltsis-Mortari A, Blazar BR, Serody JS (2005) Leukocyte migration and graft-versus-host disease. Blood 105 (11):4191-4199. doi:10.1182/blood-2004-12-4726

29. Beschorner WE, Saral R, Hutchins GM, Tutschka PJ, Santos GW (1978) Lymphocytic bronchitis associated with graft-versus-host disease in recipients of bone-marrow transplants. N Engl J Med 299 (19):1030-1036. doi:10.1056/NEJM197811092991902

30. Bolanos-Meade J, Ioffe O, Hey JC, Vogelsang GB, Akpek G (2005) Lymphocytic pneumonitis as the manifestation of acute graft-versus-host disease of the lung. Am J Hematol 79 (2):132-135. doi:10.1002/ajh.20315

31. Liu QF, Luo XD, Ning J, Xu D, Fan ZP, Sun J, Zhang Y, Xu B, Wei YQ (2009) Association between acute graft versus host disease and lung injury after allogeneic haematopoietic stem cell transplantation. Hematology 14 (2):63-72. doi:10.1179/102453309X385142

32. Teshima T, Ordemann R, Reddy P, Gagin S, Liu C, Cooke KR, Ferrara JL (2002) Acute graft-versus-host disease does not require alloantigen expression on host epithelium. Nat Med 8 (6):575-581. doi:10.1038/nm0602-575

33. Li M, Davey GM, Sutherland RM, Kurts C, Lew AM, Hirst C, Carbone FR, Heath WR (2001) Cell-associated ovalbumin is cross-presented much more efficiently than soluble ovalbumin in vivo. J Immunol 166 (10):6099-6103

34. Miyagawa F, Gutermuth J, Zhang H, Katz SI (2010) The use of mouse models to better understand mechanisms of autoimmunity and tolerance. J Autoimmun 35 (3):192-198. doi:10.1016/j.jaut.2010.06.007

35. Weinzierl AO, Lemmel C, Schoor O, Muller M, Kruger T, Wernet D, Hennenlotter J, Stenzl A, Klingel K, Rammensee HG, Stevanovic S (2007) Distorted relation between mRNA copy number and corresponding major histocompatibility complex ligand density on the cell surface. Mol Cell Proteomics 6 (1):102-113. doi:10.1074/mcp.M600310-MCP200

36. Azukizawa H, Kosaka H, Sano S, Heath WR, Takahashi I, Gao XH, Sumikawa Y, Okabe M, Yoshikawa K, Itami S (2003) Induction of T-cell-mediated skin disease specific for antigen transgenically expressed in keratinocytes. Eur J Immunol 33 (7):1879-1888. doi:10.1002/eji.200323630

37. Pilon CB, Petillon S, Naserian S, Martin GH, Badoual C, Lang P, Azoulay D, Piaggio E, Grimbert P, Cohen JL (2014) Administration of low doses of IL-2 combined to rapamycin promotes allogeneic skin graft survival in mice. Am J Transplant 14 (12):2874-2882. doi:10.1111/ajt.12944

38. Koestner W, Hapke M, Herbst J, Klein C, Welte K, Fruehauf J, Flatley A, Vignali DA, Hardtke-Wolenski M, Jaeckel E, Blazar BR, Sauer MG (2011) PD-L1 blockade effectively restores strong graft-versus-leukemia effects without graft-versus-host disease after delayed adoptive transfer of T-cell receptor gene-engineered allogeneic CD8+ T cells. Blood 117 (3):1030-1041. doi:10.1182/blood-2010-04-283119

39. Hulsdunker J, Zeiser R (2015) Insights into the pathogenesis of GvHD: what mice can teach us about man. Tissue Antigens 85 (1):2-9. doi:10.1111/tan.12497

Figures and legends

Fig. 1

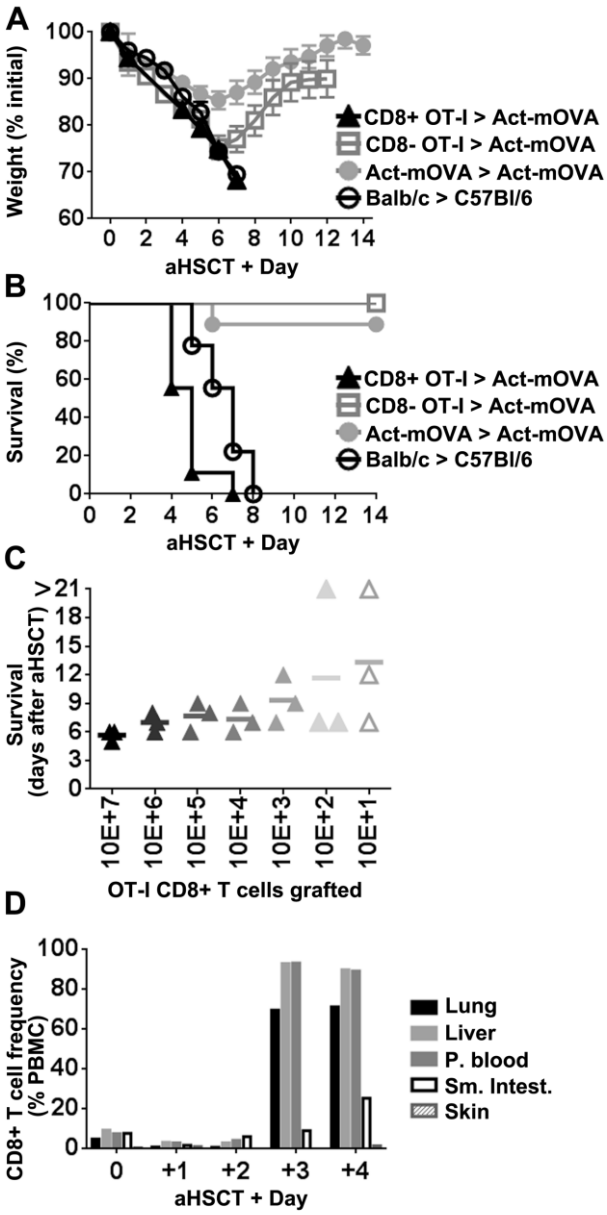

Gross pathology of an aGvHD-like disease developed by C57Bl/6 Act-mOVA mice receiving aHSCT from C57Bl/6 OT-I animals.

Percent weight loss (A), percent survival (B), length of survival depending on grafted CD8+ T cell numbers (C), and extent of CD8+ T cell infiltration observed in the small intestine, lungs and liver (D) of lethally irradiated C57Bl/6 Act-mOVA mice grafted with C57Bl/6 OT-I CD8+ T cells (CD8+ OT-I → Act-mOVA). In control experiments, Act-mOVA mice received CD8+ T cell-depleted grafts (CD8- OT-I → Act-mOVA), autografts (Act-mOVA → Act-

mOVA). Typical disease course observed in a standard murine aGVHD model with multiple MHC and minor allele disparities is shown as reference (Balb/c → C57Bl/6, all n≥9).

Fig. 2

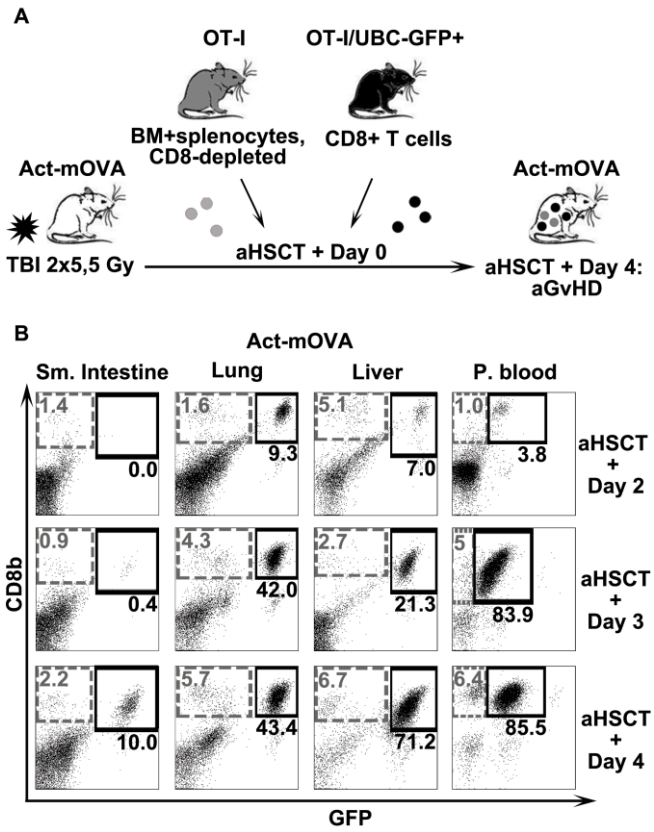

Assessment of graft UBC-GFP/OT-I CD8+ T cell infiltration into various organs of a GFP-negative Act-mOVA host after aHSCT

A) Preparation of an UBC-GFP/OT-I CD8+ T cell-graft allow discrimination between graft CD8+ T cells and any other T cells of the graft or the recipient by GFP labeling. B). Flow cytometric follow-up analysis of the frequency of GFP negative host CD8+ T cells (left, grey boxes) as compared to UBC-GFP/OT-I graft CD8+ T cell infiltration (right, black boxes) in various organs of Act-mOVA mice in three different time points after aHSCT, as indicated. Numbers indicate percent frequency of the given subset within all PBMCs.

Fig. 3

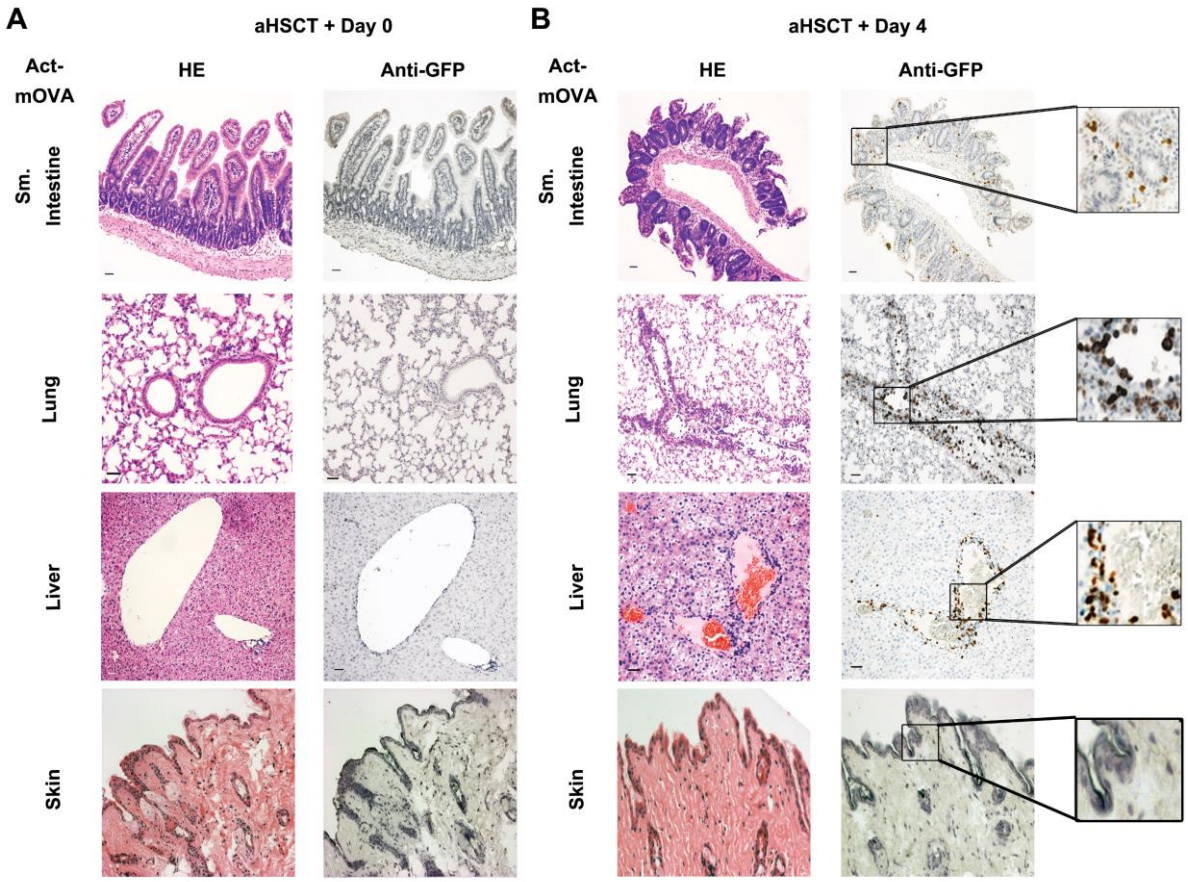

Simultaneous analysis of graft UBC-GFP/OT-I CD8+ T cell distribution and disease pathology in typical target organs of aGvHD

Representative images of HE-staining and anti-GFP IHC performed on skin, liver, lung and small intestinal tissue sections of Act-mOVA mice grafted with UBC-GFP/OT-I CD8+ T cells on the day of aHSCT (A, aHSCT + Day 0, left, controls) and the day preceding median survival (B, aHSCT + Day 4, right, aGvHD). For clarity, magnified images (far right, black boxes) aid identification of graft UBC-GFP/OT-I CD8+ T cells (brown dots) within the analyzed organs. Scale bars: 50 µm (on each panel, bottom, left).

Fig. 4

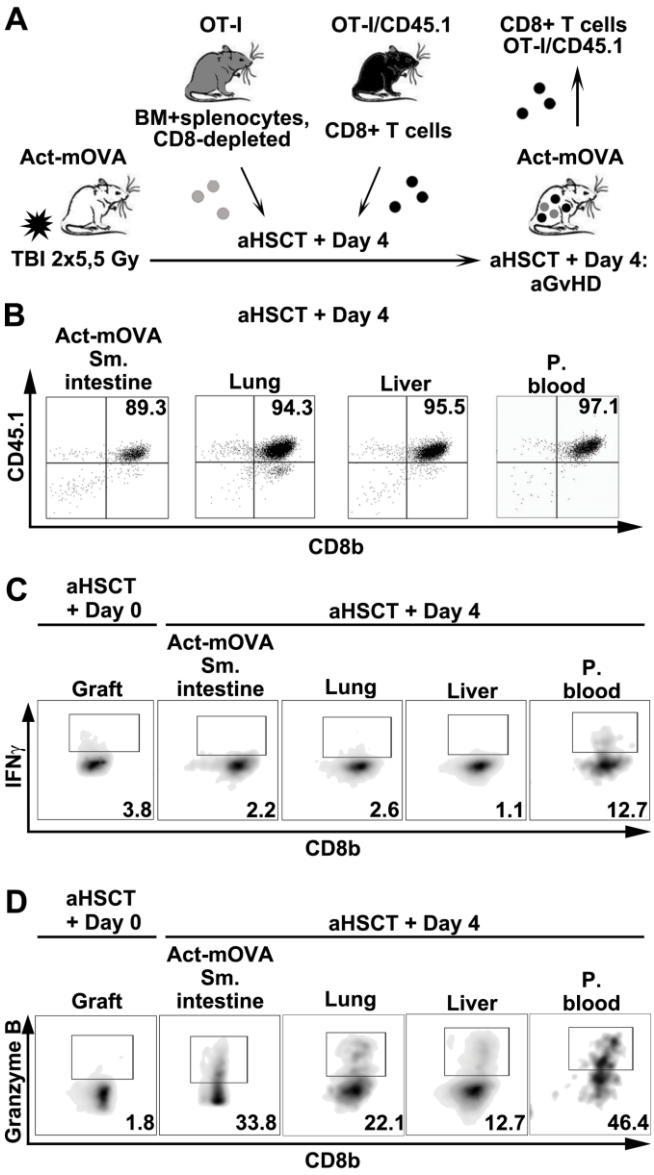

Selective re-isolation and flow cytometric analysis of CTL effector molecule production in graft CD45.1/OT-I CD8+ T cells retrieved from various organs of Act-mOVA recipients affected by aGVHD

(A) Preparation of a CD45.1/OT-I CD8+ T cell-spiked graft allowing selective retrieval of graft CD8+ T cells from various organs of an aGVHD-affected recipient for downstream functional studies. (B) Selective re-isolation of CD45.1-labeled CD8+ OT-I T cells of the graft from various tissues of the host by automated tissue dissociation and subsequent magnetic sorting. (C) Intracellular granzyme B and (D) interferon gamma staining of graft

CD45.1/OT-I CD8+ T cells re-isolated from the graft, right before graft administration (aHSCT + Day 0), and various organs of an aGVHD-affected Act-mOVA host (aHSCT + Day 4).

Fig. 5

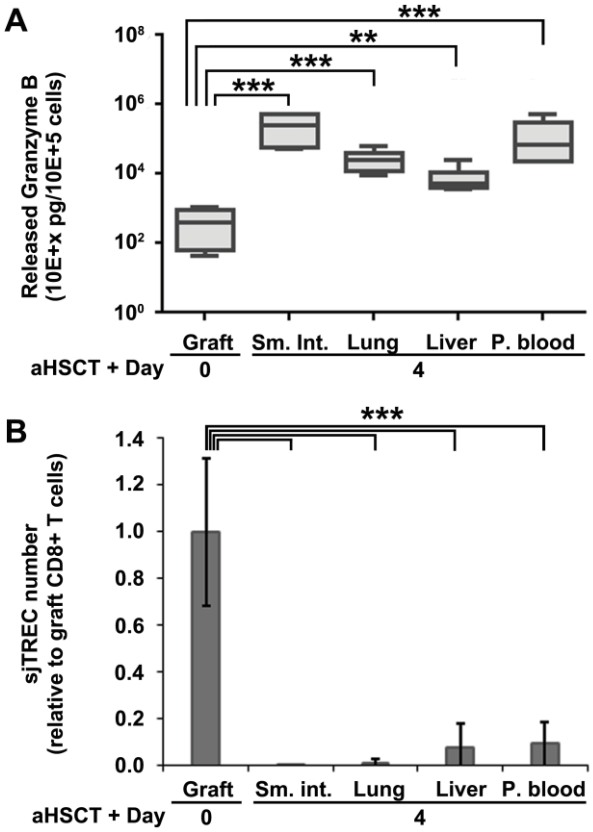

Gradual loss of naïve-derived T cell receptor excision circles (TRECs) and induction of granzyme B release in CD45.1/OT-I CD8+ T cells grafted into Act-mOVA recipients to induce aGvHD

A) Assessment of granzyme B release by ELISA in graft CD45.1/OT-I CD8+ T cells before aHSCT (aHSCT + Day 0), and graft CD45.1/OT-I CD8+ T cells retrieved from various organs of Act-mOVA hosts shortly before succumbing to aGvHD (aHSCT + Day 4). B) Q-PCR assessment of TREC numbers present in the same samples. Stars indicate significant differences, group size is n=5 in all groups shown.

Fig. 6

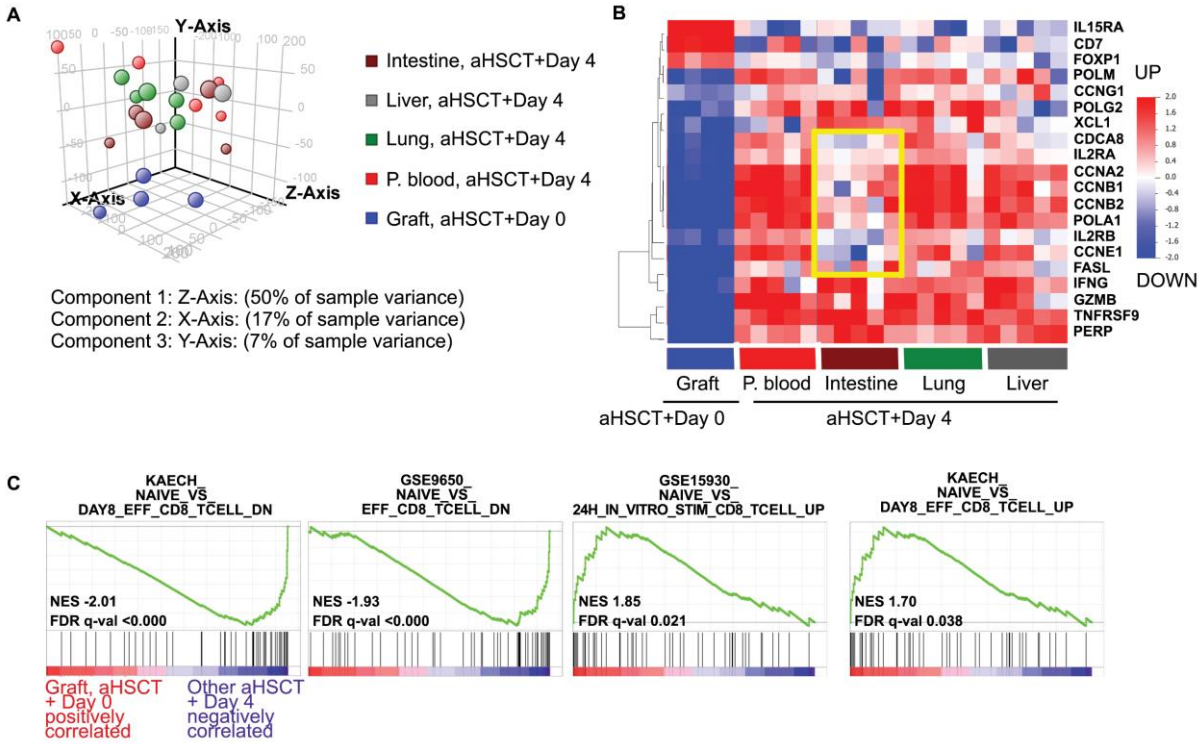

Gene expression profiling of graft CD45.1/OT-I CD8+ T cells before and four days after grafting into Act-mOVA recipients to induce aGvHD

A) Three dimensional principal component analysis of sample variance based on gene expression profiling. CD45.1/OT-I CD8+ T cells isolated from the graft, before grafting, and various organs of the host, four days later, are shown color coded, as indicated. The first three components of global sample variance are displayed by the three axes of the 3D plot; % of total variance covered by each axis is also indicated. B) Heatmap displaying standardized gene expression patterns of twenty selected, differentially expressed genes closely associated with naïve to effector transition in grafted CD45.1/OT-I CD8+ T cells. Shades of red indicate up-, shades of blue downregulation. Genes are identified by HUGO gene symbols. C) Gene set enrichment analysis (GSEA) of the same dataset. Enrichment plots display distribution of genes among significantly enriched gene sets of Broad Institute's MSig Database showing the strongest observed correlation with the phenotype of grafted CD45.1/OT-I CD8+ T cells on aHSCT + Day 0 vs Day 4. NES, normalized enrichment score; FDR q-val, estimated probability of false discovery rate.

Supplementary Figure 1: Successful elimination host CD8+ T cells by lethal dose TBI.

Grafting CD45.1 bone marrow into CD45.2 hosts following lethal dose TBI confirms successful elimination of host CTLs by Day 7. Full replacement of host CTLs with graft-derived CTLs occurs by aHSCT + Day 14. Representative flow cytometric analysis of the peripheral blood of affected animals.

Supplementary Table 1: Differentially expressed genes discriminating between CD45.1/OT-I CD8+ T cells grafted into Act-mOVA mive before (aHSCT + Day 0) and four days after grafting (aHSCT + Day 4).

Table of 2514 genes differentially expressed by CD45.1/OT-I CD8+ T cells in the graft (aHSCT + Day 0), and graft-derived T cells infiltrating the small intestine, lung and liver of Act-mOVA recipients four days later (aHSCT + Day 4). Agilent microarray probeset IDs, HUGO Gene Symbols, uncorrected and Benjamini-Hochberg corrected results of One-Way ANOVA followed by Tukey's all pairwise analysis, p-values, fold-changes, gene names, full gene annotations and Agilent probeset descriptions are shown.